Tuning the photoelectrochemical properties of hierarchical TiO_2 nanostructures by control of pulsed laser deposition and annealing in reducing conditions

Luca Mascaretti[a,*], Roberto Matarrese[b], Andrea Ravanelli[b], Manuel Isacchi[b], Piero Mazzolini[a,c], Carlo S. Casari[a,c], Valeria Russo[a], Isabella Nova[b], Giancarlo Terraneo[d], Caterina Ducati[e], Andrea Li Bassi[a,c,*]

[a] Micro- and Nanostructured Materials Laboratory, Department of Energy, Politecnico di Milano, via Ponzio 34/3, 20133, Milano, Italy.

[b] Laboratory of Catalysis and Catalytic Processes, Department of Energy, Politecnico di Milano, via La Masa 34, 20156, Milano, Italy.

[c] Center for Nanoscience and Technology – IIT@Polimi, via Giovanni Pascoli 70/3, 20133, Milano, Italy.

[d] Laboratory of Supramolecular and BioNano Materials (SupraBioNanoLab), Department of Chemistry, Materials and Chemical Engineering "Giulio Natta", Politecnico di Milano, via L. Mancinelli 7, 20131, Milano, Italy.

[e] Department of Materials Science & Metallurgy, University of Cambridge, 27 Charles Babbage Road, CB3 0FS, Cambridge, UK.

***corresponding author**

Andrea Li Bassi
Micro- and Nanostructured Materials Laboratory, Department of Energy, Politecnico di Milano
Via Ponzio 34/3, 20133, Milano, Italy
andrea.libassi@polimi.it

Luca Mascaretti
Micro- and Nanostructured Materials Laboratory, Department of Energy, Politecnico di Milano
Via Ponzio 34/3, 20133, Milano, Italy
luca.mascaretti@polimi.it

Abstract

Nanostructured TiO_2 films with hierarchical morphology were synthesized by Pulsed Laser Deposition (PLD) and tested as photoanodes for photoelectrochemical water splitting. The tuning of their photoresponse was addressed by employing oxygen-poor conditions both during the growth and the post-deposition annealing of the material: depositions were performed in different Ar/O_2 background gas mixtures from both TiO_2 and Ti targets, while thermal treatments, after standard air annealing for crystallization, were performed in a Ar/H_2 mixture. By testing the double-annealed photoanodes in a three-electrode cell with solar simulator illumination, clear trends with optimal synthesis conditions for each target material appeared; for these conditions, also the effect of vacuum annealing was studied. The morphological, structural and optical properties were investigated by SEM, Raman spectroscopy and UV-visible-IR spectroscopy. From these observations, it emerged that the films deposited in the presence of oxygen do not show substantial differences in their morphology/structure, on the contrary of pure Ar-deposited films; thus, the trends in photoresponse can be related to differences in the defect concentration of the material, induced by depositions in the different Ar/O_2 atmospheres and by annealing in Ar/H_2 mixture or vacuum. In particular, the reported results suggest that some degree of oxygen shortage in the deposition process leads to a better photoelectrochemical performance, and a combination between improved charge transport and surface hydrogenation/reduction effect, leading to enhanced photoresponse, is suggested. This work elucidates the possibility of an accurate tuning of the material photoactivity by control of the deposition and annealing conditions.

Keywords

TiO_2; hierarchical nanostructures; pulsed laser deposition; photoelectrochemical water splitting; reducing deposition/annealing conditions.

1. Introduction

Since the pioneering work by Fujishima and Honda [1], titanium dioxide (TiO_2) has been extensively studied as photocatalytic material for hydrogen production by water splitting [2–4]. However, this material still shows intrinsic limitations, such as a light absorption process basically restrained just to the UV range and a limited quantum efficiency for the water splitting process. For this reason, many efforts are still being carried out to improve its performance. Several experimental approaches have been proposed to overcome TiO_2 intrinsic limitations: i) exploitation of nanostructured morphologies such as nanotubes [5,6] and hierarchical nanostructures [7], to increase the active surface, minimize charge recombination and manage light scattering; ii) introduction of extrinsic dopants or sensitization [8], to shift absorption towards the visible range; iii) introduction of surface disorder and/or intrinsic defects (oxygen vacancies, Ti interstitials) with thermal treatments in hydrogen or other reducing atmospheres [9,10], to increase the photocatalytic activity; iv) integration with noble metal plasmonic nanoparticles [11,12], to harvest photons in the visible range or increase the generation of electron/hole pairs in the semiconductor; v) combination with co-catalysts, to favour the charge separation [13,14]. In addition, TiO_2 has also been employed in combination with other photoactive materials as protective layer [15,16] or interlayer for increasing the charge collection [17–19].

One-dimensional (1D) or quasi-1D nanostructured forms of TiO_2 are particularly interesting due to their possibility to preferentially transport the photogenerated electrons towards the back-contact [20,21]. From the synthesis point of view, among several physical vapor deposition techniques, Pulsed Laser Deposition (PLD) enables to tune the morphological, structural, chemical and functional properties of the deposited materials by properly adjusting the process parameters [22,23]. Thanks to these advantages, some of us and other groups have exploited this technique to synthesize hierarchical TiO_2 nanomaterials and study their application as photoanodes for dye-sensitized solar cells [24–26], for photocatalysis experiments [27] and for photoelectrochemical (PEC) water splitting [28–30].

1D nanostructures have been recently combined with surface disorder/defects by performing hydrogenation/reduction treatments [10] after the encouraging results obtained with TiO_2 nanopowders [9]; for instance, rutile nanowires have shown extensive photocurrent enhancement after hydrogen annealing at 350°C [31]. Based on these results and on the morphological peculiarity of vertically-oriented, hierarchical TiO_2 nanostructures prepared by PLD, we have recently studied their hydrogenation/reduction both during deposition and post-annealing steps [32]. We found that deposition in oxygen-poor conditions was critical to obtain a significant enhancement of photoactivity of the film, when followed by a double thermal treatment (in air and then in Ar/H_2); this was ascribed to defects introduced both by the deposition atmosphere as well as by the annealing treatments. Consequently, in order to obtain a more precise and effective tuning of the material photoactivity, it is mandatory to investigate more in detail the role of oxygen during deposition and the role of the annealing atmosphere, such as vacuum as an alternative to Ar/H_2 mixture [33,34].

For these reasons, in this work we extensively investigate the effect of deposition parameters (target material, i.e. TiO_2 or metal Ti, and atmosphere composition, i.e. oxygen content) and, for selected

samples, of the annealing atmosphere (Ar/H_2 mixture at atmospheric pressure or vacuum) on the structure and photoresponse of PLD-deposited TiO_2 hierarchically grown photoanodes.

2. Experimental

2.1 Synthesis of TiO_2 photoanodes

TiO_2 nanostructured films have been deposited by ablating a TiO_2 (99.9%) or Ti (99.99%) target with a ns-pulsed laser (Nd:YAG, 2nd harmonic, λ = 532 nm, repetition rate 10 Hz, pulse duration 5-7 ns). The laser fluence on the target was set at about 3.5 J/cm^2 and the laser pulse energy was 170 mJ. Silicon (100), soda-lime glass and titanium plates were used as substrates, mounted on an off-axis rotating sample holder at a fixed target-to-substrate distance of 50 mm. The depositions were all performed at room temperature. Titanium plate substrates of 2×1 cm^2 were half masked during deposition in order to leave a clean surface for the electrical contacts of the photoelectrochemical measurements. The depositions were performed at a fixed background gas pressure of 5 Pa in different Ar/O_2 mixtures, from pure O_2 to pure Ar, as illustrated in Table 1. The nominal film thickness was set at about 1300 nm (the actual thickness, measured by SEM, varied between 1000 and 1400 nm). The deposited mass ranged between 0.15 and 0.35 mg/cm^2, as estimated from quartz microbalance measurements, and the deposition rate ranged between 3 and 11 nm/min, depending on the specific conditions.

Table 1: set of the different deposition conditions explored and corresponding sample names.

Atmosphere	**TiO_2 target**	**Ti target**
100% O_2	O_2-TiO_2	O_2-Ti
75% O_2, 25% Ar	Ar/O_2 (25:75)-TiO_2	Ar/O_2 (25:75)-Ti
50% O_2, 50% Ar	Ar/O_2 (50:50)-TiO_2	Ar/O_2 (50:50)-Ti
25% O_2, 75% Ar	Ar/O_2 (75:25)-TiO_2	Ar/O_2 (75:25)-Ti
100% Ar	Ar-TiO_2	Ar-Ti

According to the results of our previous work [32], two kinds of annealing treatments were performed ex-situ on the samples: a reference air annealing in a Lenton muffle furnace (4°C/min heating ramp, 2 hours dwell at 500°C), hereinafter labelled as **[Air]**, and a double annealing, i.e. air annealing followed by a thermal treatment in an Ar/H_2 (97%-3%) mixture at atmospheric pressure in a home-made furnace (10°C/min heating ramp, 3 hours dwell at 500°C), labelled as **[Air+Ar/H_2]**. In addition, for the thin films showing the highest photoresponse (as shown in the Results section), the second step in Ar/H_2 mixture was substituted with a thermal treatment with the same temperature program in vacuum ($P < 3\times10^{-4}$ Pa), labelled as **[Air+Vac]**.

2.2 Morphological, structural and optical characterization

SEM analyses (top view and cross-sectional) were performed on samples grown on silicon substrates with a ZEISS Supra 40 FEG-SEM without any sample preparation.

TEM images were acquired using a FEI Tecnai F20 microscope operated at 200 kV and equipped with a OneView camera.

Raman spectra were collected from samples grown on silicon or glass substrates using a Renishaw InVia micro Raman spectrophotometer with 514.5 nm laser excitation wavelength and power on the sample of about 1 mW.

X-Ray diffraction patterns were collected using a Bruker D8 Adavance X Ray diffractometer, operating in reflection mode with Ge-monochromated Cu Kα1 radiation (λ = 1.5406 Å) and a linear position-sensitive detector; with a 2θ range 10−70°, a step size 0.038° and time/step 1.5 sec. Samples were mounted in sample holder with motorized z-position (4.3 mm). Diffraction patterns were collected at room temperature. The peak position and the full-width at half maximum height (FWHM) of the peaks were then obtained using TOPAS software (Bruker). The crystallite sizes were estimated through the Scherrer formula [35].

Optical transmittance (in the range 250 – 2000 nm) and reflectance spectra (in the range 290 – 600 nm) were evaluated with a UV-vis-NIR PerkinElmer Lambda 1050 spectrophotometer with a 150 mm diameter integrating sphere. All the acquired spectra were normalized with respect to the glass substrate contribution by setting to 1 the intensity at the glass/film interface.

2.3 Photoelectrochemical experiments

Photoelectrochemical (PEC) measurements were carried out in aqueous KOH solution (0.1 M) with a three-electrode cell equipped with a flat quartz window. TiO_2 films on Ti substrate photoanodes (working area of 1 cm^2) were used as the working electrode while a platinum grid and a saturated calomel electrode (SCE) were used as counter and reference electrode, respectively. The light source was a solar simulator (Lot Quantum Design LS0306) equipped with a 300 W xenon arc lamp and AM1.5G filter (Lot Quantum Design LSZ389). The incident light intensity was measured prior to the experiments using a light meter HD2302.0 (Delta OHM). The performance of the TiO_2 photoanodes was evaluated by measuring the photocurrents under an external bias [36–39], provided by a potentiostat (Amel 7050) performing potential ramps from −0.8 V to about 0.5 V, with a scan rate of 5 mV/s. PEC measurements were also performed under constant light illumination and fixed bias potential (0.4 V) for 6 hours, in order to evaluate the photoanodes' stability [40–42].

3. Results and discussion

3.1 Photoelectrochemical response

In search of a photoresponse optimization of TiO_2 nanostructured films prepared by PLD for water splitting applications, all the photoanodes presented in Table 1 were tested in a photoelectrochemical cell in the presence of 0.1 M KOH electrolyte.

Fig. 1 shows the photocurrent results for films deposited from TiO_2, annealed in [Air+Ar/H_2] (Fig. 1A) and in [Air] (Fig 1B) in all the investigated Ar/O_2 mixtures. The photocurrent density values reported in Figs. 1A and B were used to calculate the photoconversion efficiency (η%) according to equation (1), which takes into account not only the power light, but also the external potential applied to the electrode [43]:

$$\eta(\%) = \frac{J(E^0 - |E_{app}|)}{I} \times 100 \quad (1)$$

where J is the photocurrent density (μA cm^{-2}), $E°$=1.23 V is the standard reversible potential for water splitting, $|E_{app}|$ is the external applied potential, evaluated as the difference between the measured pontential (V) vs. SCE and the Open Circuit Voltage (OCV) under the irradiated power light, and I is the incident light power density (96000 μW cm^{-2}). Figs. 1C and D show the variation of η(%) as a function of the measured potential for films annealed in [Air+Ar/H_2] and in [Air], respectively.

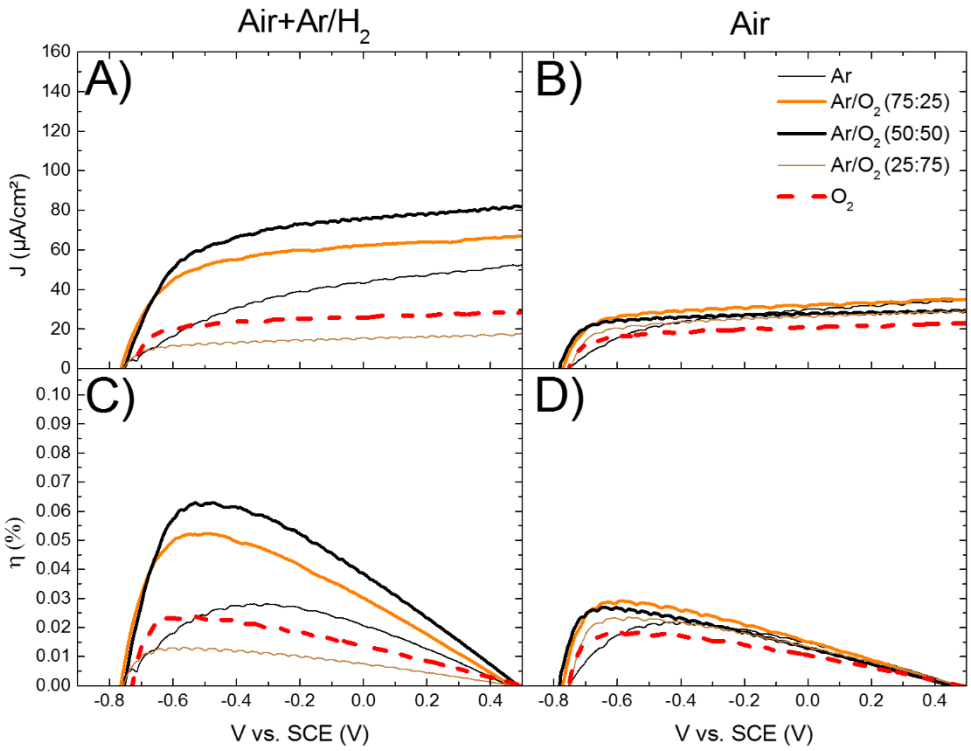

Figure 1: Effect of the deposition atmosphere on the performances for photoanodes prepared starting from TiO_2 target annealed with [Air+Ar/H_2] (**A** and **C**) and with [Air] (**B** and **D**): photocurrents (**A** and **B**) and photoconversion efficiencies (**C** and **D**) results. The legend placed in **B** refers to all the subfigures.

As expected, all the films exhibit negligible anodic photocurrents (less than 5 μA/cm^2) under dark conditions (not shown) over the whole investigated potential range, indicating that negligible photoelectrochemical water oxidation occurs at the anode surface. On the contrary, under

illumination, photocurrent generation is recorded because of the efficient charge carriers (i.e. electron-holes pairs) generation from the incident light and the subsequent water oxidation occurring at the photoanodes by holes.

In the case of films deposited from TiO_2 target and then annealed in [Air+Ar/H_2] (Fig. 1A) the photocurrent onset potential is observed near −0.75 V; then the photocurrent density gradually increases with the applied potential because of the increased charge carriers separation under the effect of the applied bias [44–46]. The films deposited with the highest oxygen contents (i.e. 100 and 75% O_2) in the background atmosphere show the lowest photoresponse: low photocurrent densities are measured through all the potential window, i.e. reaching values near 30 and 20 μA cm^{-2} at 0.5 V, respectively. The photoresponse increases for films deposited with lower oxygen amounts (i.e. 50 and 25% O_2): higher photocurrent densities are measured in the whole potential range, i.e. reaching values near 80 and 70 μA cm^{-2} at 0.5 V, respectively. Besides, deposition in pure Ar (i.e. Ar-TiO_2-[Air+Ar/H_2]) results in a significant decrease of the photoresponse, with a photocurrent density of about 50 μA cm^{-2} at 0.5 V and a different shape of the photocurrent characteristic. This outcome indicates, for films deposited from TiO_2 target, the existence of an optimal O_2 concentration (i.e. 25-50% O_2) in the deposition atmosphere leading to an improved photoactivity. This is confirmed by the corresponding photoconversion efficiencies, plotted in Fig. 1C. Indeed, the highest photoconversion efficiencies are measured for the Ar/O_2 (50:50) and Ar/O_2 (75:25) films, i.e. near 0.06 and 0.05%, respectively.

Considering the films deposited from TiO_2 target and then annealed in [Air] (Fig. 1B), the photoresponse is significantly lower than those annealed in [Air+ArH_2]. In fact, for all samples, low photocurrent densities are measured through all the potential window, i.e. approaching values in the range of 20-35 μA cm^{-2} at 0.5 V. Nevertheless, also in this case the highest photoconversion efficiencies are measured for the Ar/O_2 (50:50) and Ar/O_2 (75:25) films, i.e. near 0.03 %.

In the case of photoanodes prepared from Ti target with annealing in [Air+Ar/H_2] (Fig. 2A), different trends of photoactivity as a function of preparation conditions are observed, if compared to those deposited from TiO_2. For the Ar/O_2 (75:25)-Ti-[Air+Ar/H_2] and Ar/O_2 (50:50)-Ti-[Air+Ar/H_2] films, the photocurrent onset potential is observed at about −0.8 V (i.e. lower than films deposited from TiO_2 target) and photocurrent density reaching a value near 60 μA cm^{-2} at 0.5 V is measured. The photoresponse increases for samples deposited in oxygen-rich mixtures (i.e. Ar/O_2 (25:75)-Ti-[Air+Ar/H_2] and O_2-Ti-[Air+Ar/H_2] photoanodes) for which the highest photocurrent results are achieved, i.e. reaching values near 120 and 110 μA cm^{-2} at 0.5 V, respectively. In this case, the negative shift of the photocurrent onset, together with the higher photocurrent response, indicate a more efficient generation and transfer of photogenerated charge carriers and minor recombination losses, as well [47–49]. Accordingly, the highest photoconversion efficiencies of ca. 0.1 and 0.09% are obtained (see Fig. 1D). The film deposited in pure argon (i.e. Ar-Ti-[Air+Ar/H_2]) instead shows a photocurrent onset potential near −0.65 V and a photocurrent density gradually increasing with the applied potential up to ca. 35 μA cm^{-2} at 0.5 V; the qualitative different behavior of this film should be related to the different morphology, crystallinity and composition of this sample, as discussed in the following (see Section 3.2).

Of note, also for films deposited from Ti target and then annealed in [Air] (Fig. 2B) the photoresponse is significantly lower than those annealed in [Air+ArH_2], but the same trends of

photoactivity as a function of preparation conditions are observed. Accordingly, samples deposited in oxygen-rich mixtures (i.e. Ar/O_2 (25:75)-Ti-[Air+Ar/H_2] and O_2-Ti-[Air+Ar/H_2] photoanodes) achieve the highest photoconversion efficiencies of ca. 0.05%. Conversely the sample deposited in pure argon shows the lowest values of maximum efficiencies, i.e. near 0.02%.

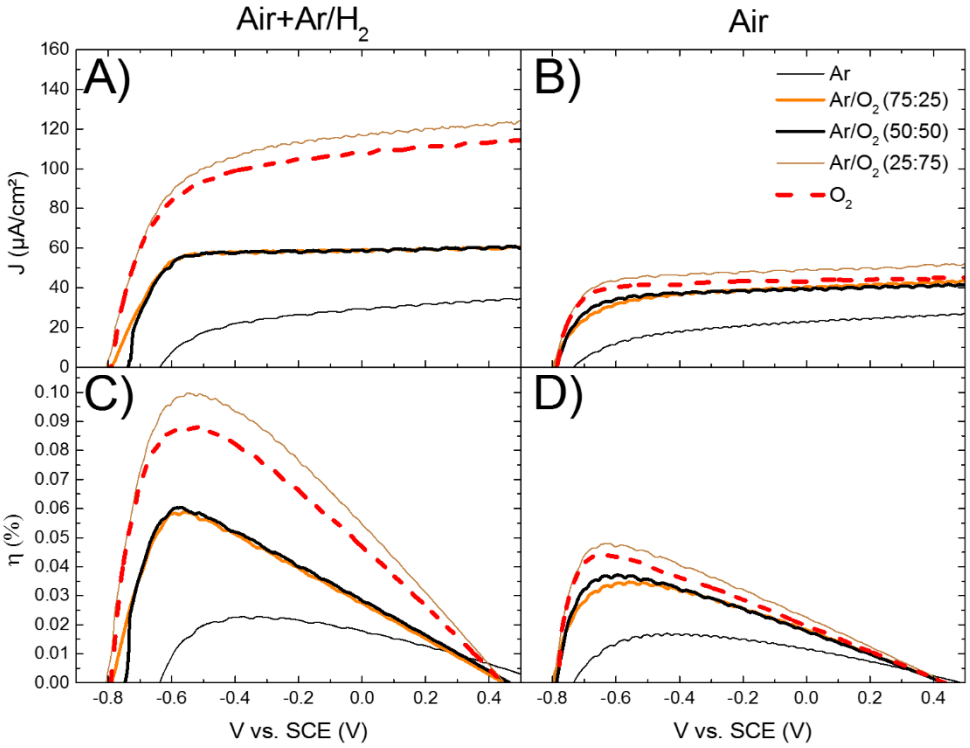

Figure 2: Effect of the deposition atmosphere on the performances for photoanodes prepared starting from Ti target annealed with [Air+Ar/H_2] (**A** and **C**) and with [Air] (**B** and **D**): photocurrents (**A** and **B**) and photoconversion efficiencies (**C** and **D**) results. The legend placed in **B** refers to all the subfigures.

In the literature, only a few examples concerning the hydrogenation of TiO_2 in Ar/H_2 or N_2/H_2 mixture at atmospheric pressure have been reported (instead of the more investigated high purity H_2 treatment); in these cases a photoresponse enhancement with respect to air annealing has already been reported [50–56]. For instance, the photocurrent values reported in ref. [54] are the closest to our study; however, a direct comparison between these values is not straightforward due to differences in experimental conditions (e.g. electrolyte, illumination) or in material properties (e.g. thickness, crystalline phase, morphology).

In order to analyze the above results more in detail, the maximum photoconversion efficiency values are reported in Fig. 3A as a function of the different deposition background gas mixtures for films deposited from both TiO_2 and Ti targets. Of note, photocurrent measurements were repeated over several months, obtaining very similar results as those presented in Figs. 1 and 2 (not shown) which indicates the good reproducibility of the experiments and provides a first indication of the sample structural stability as well as performance stability for PEC water splitting. Accordingly, the data points and error bars in Fig. 3A depict the average and standard deviation values over at least six measurements.

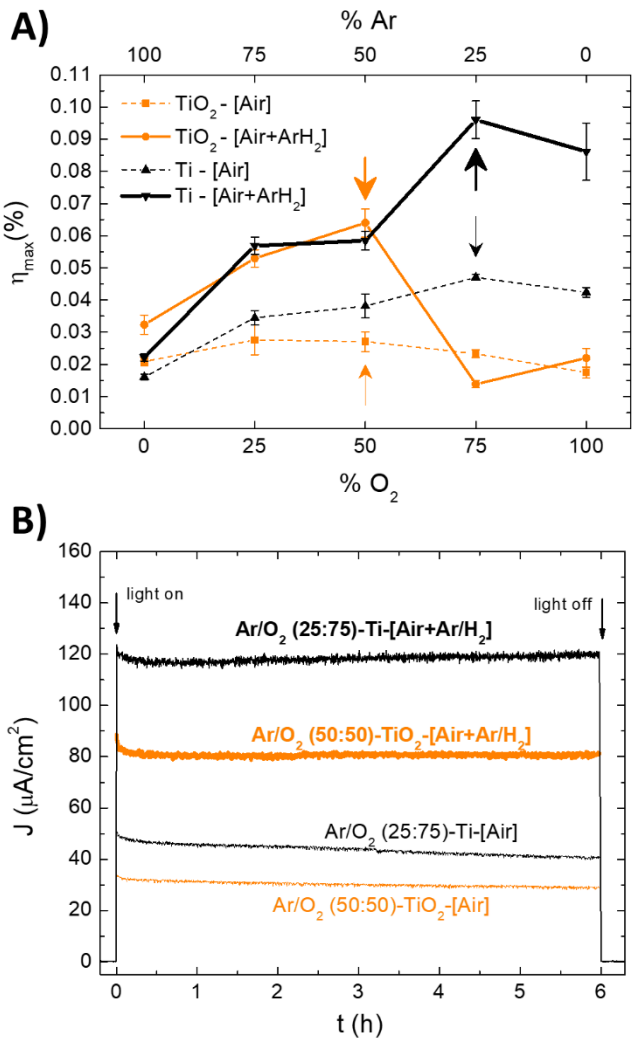

Figure 3: A) Effect of the deposition atmosphere (i.e. from pure O_2 to pure Ar) on the maximum photoconversion efficiency for photoanodes prepared from TiO_2 target annealed in [Air] (dotted-orange) and in [Air+Ar/H_2] (solid-orange) and from Ti target annealed in [Air] (dotted-black) and in [Air+Ar/H_2] (solid-black). **B)** Photostability of the optimal photoanodes, marked with an arrow in **A**, measured by photocurrent over time with applied bias potential of 0.4 V vs SCE.

Considering the films deposited from Ti target, Fig. 3A points out that the photoresponse increases upon increasing the oxygen content in the deposition atmosphere up to the 75%, both for films annealed in [Air] and in [Air+Ar/H_2]. Besides, it is clear that photoanodes annealed in [Air+Ar/H_2] outperform those annealed in [Air]. In the case of films deposited from TiO_2 target, the photoresponse is maximized for a 50% oxygen content in the deposition atmosphere; again, the photoactivity is higher for films annealed in [Air+Ar/H_2] than for those annealed in [Air]. Considering the target effect, the best performing films deposited from Ti target (i.e. prepared in O_2-rich atmospheres and with [Air+Ar/H_2] annealing) show higher photoactivities than those deposited from TiO_2 target.

The photostability of the Ar/O_2 (50:50)-TiO_2-[Air+Ar/H_2] and Ar/O_2 (25:75)-Ti-[Air+Ar/H_2] films (i.e. the photoanodes that showed the best performances) was further investigated. Fig. 3B shows the photocurrents measured over six hours with applied bias potential of 0.4 V. As it clearly appears, under dark conditions (before $t = 0$ and after $t = 6$ h) negligible photocurrents are observed, indicating that no reaction occurred at the photoanodes in the absence of light

illumination. On the contrary, under irradiation, photocurrent evolution is observed as a result of water oxidation occurring at the photoanodes. In line with the above results, the film deposited from Ti target shows a higher photoresponse than that deposited from TiO_2: as a matter of fact, upon illumination (at $t = 0$), the current densities increase at ca. 120 μA/cm^2 and 80 μA/cm^2 for the samples obtained by Ti and TiO_2 targets, respectively. Moreover, the film deposited from Ti target shows a slightly better photostability. In fact, after 6 h of continuous illumination the photocurrent drops by about 8% and 4% for films prepared from TiO_2 and Ti targets respectively. For comparison purpose, the same photostability tests were performed over the same films (i.e. Ar/O_2 (50:50)-TiO_2 and Ar/O_2 (25:75)-Ti) annealed in [Air]. In this case, a lower stability is observed: after 6 h of continuous illumination the photocurrent drops by about 17 and 19% for films prepared from TiO_2 and Ti targets, respectively.

Finally, for the most promising films (i.e. Ar/O_2 (50:50)-TiO_2 and Ar/O_2 (25:75)-Ti samples), the effect of a double [Air+Vac] thermal treatment on the photoresponse was also investigated. Figs. 4A and B show the photoresponse (in terms of photoconversion efficiencies) for films deposited from TiO_2 and Ti targets, respectively. For comparison purpose, the results obtained for the same films annealed in [Air] and [Air+Ar/H_2] are also reported. The vacuum thermal treatment shows a different effect on the photoanodes performance depending on the employed target material. A positive effect is observed for the film deposited from TiO_2 target: a maximum photoconversion efficiency close to 0.08% is obtained after the [Air+Vac] annealing, higher than that obtained after [Air+Ar/H_2] and [Air] thermal treatments (Fig. 4A). On the contrary, for the film deposited from Ti target (Fig. 4B) no increase in the photoconversion efficiency is observed with respect to the [Air]-annealed film; in addition, the efficiency values are obtained with an applied potential higher than that for the [Air]-annealed film, which is undesirable for practical application.

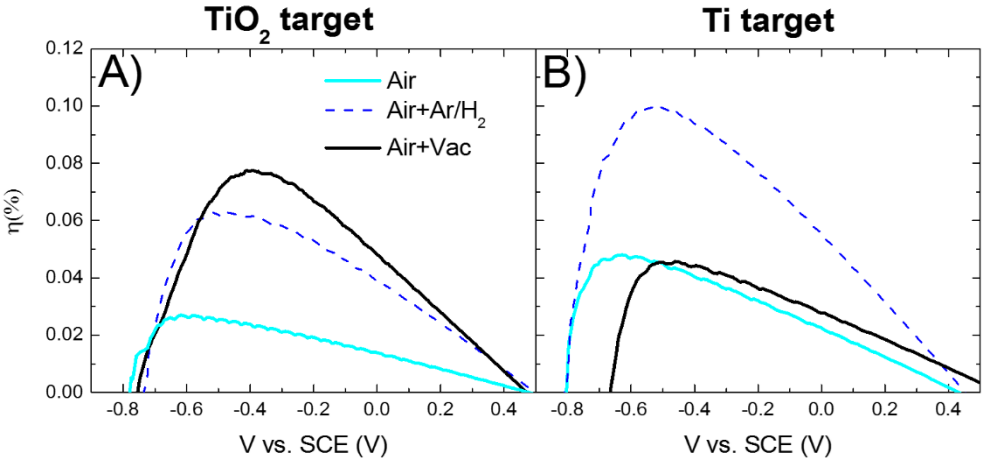

Figure 4: Photoconversion efficiency curves for Ar-O_2 (50:50)-TiO_2 **(A)** and Ar-O_2 (25:75)-Ti **(B)** photoanodes annealed in [Air] (light blue), [Air+Ar/H_2] (dotted blue), and [Air+Vac] (black).

3.2 Photoanode structure and morphology

As shown in the previous section, two optimal depositions conditions, respectively from TiO_2 and Ti target, have been found, i.e. Ar/O_2 (50:50)-TiO_2 and Ar/O_2 (25:75)-Ti. Accordingly, the full characterization of these films is presented in this section; all the other depositions in Ar/O_2 mixtures and in pure O_2 show similar morphological/structural features to the optimal ones (for further details, see Supporting Information). On the contrary, SEM and Raman spectra for pure Ar

depositions (i.e. Ar-TiO_2 and Ar-Ti films) are included, since they show a different behaviour from the other films, as discussed below.

The films grown in Ar/O_2 mixture at 5 Pa show a porous hierarchical organization, as shown in Fig. 5, and they are composed by nanoparticles, as evidenced by Fig. 6, in which higher magnification SEM images are reported. In addition, the different target material (Figs. 6A, D and 6B, E) or annealing treatments (Figs. 6A, B and 6D, E) do not globally change the overall morphology. On the other hand, films grown in Ar gas at 5 Pa are more compact (Figs. 6C and F) and exhibit a lower degree of porosity, in particular, the one deposited using the Ti target. In addition, the Ar-Ti-[Air+Ar/H_2] film (Fig. 6F) is characterized by a rougher and more irregular surface with respect to the other films.

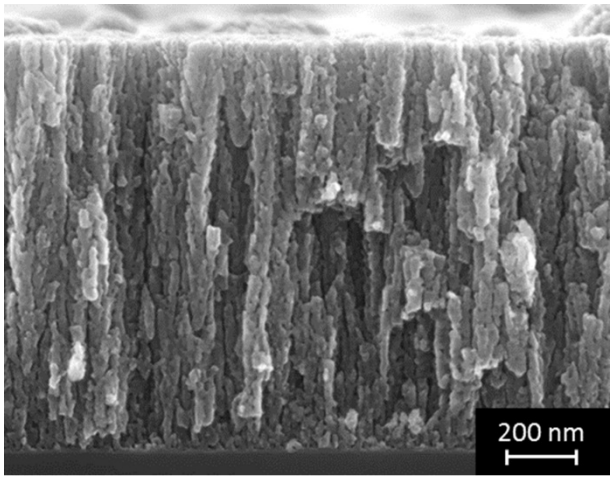

Figure 5: SEM image of Ar/O_2 (50:50)-TiO_2-[Air+Ar/H_2] sample; the whole film grown on Si substrate can be observed.

The more compact morphology obtained when depositing in pure Ar atmosphere (with respect to O_2-containing atmospheres) is in agreement with previous reports [57,58] and with optical emission spectra of the plasma plume produced by ablation of a TiO_2 target in 5 Pa of Ar, which indicate that the kinetic energy of Ti ions is higher than that of Ti ions ablated in 5 Pa of pure O_2 [59]. On the other hand, provided that some O_2 is present in the background gas (in our case at least 25%), the same hierarchical morphology of the O_2-TiO_2 film is achieved, regardless the precise relative composition of the gas atmosphere (see Figs. S1 and S2, Supporting information).

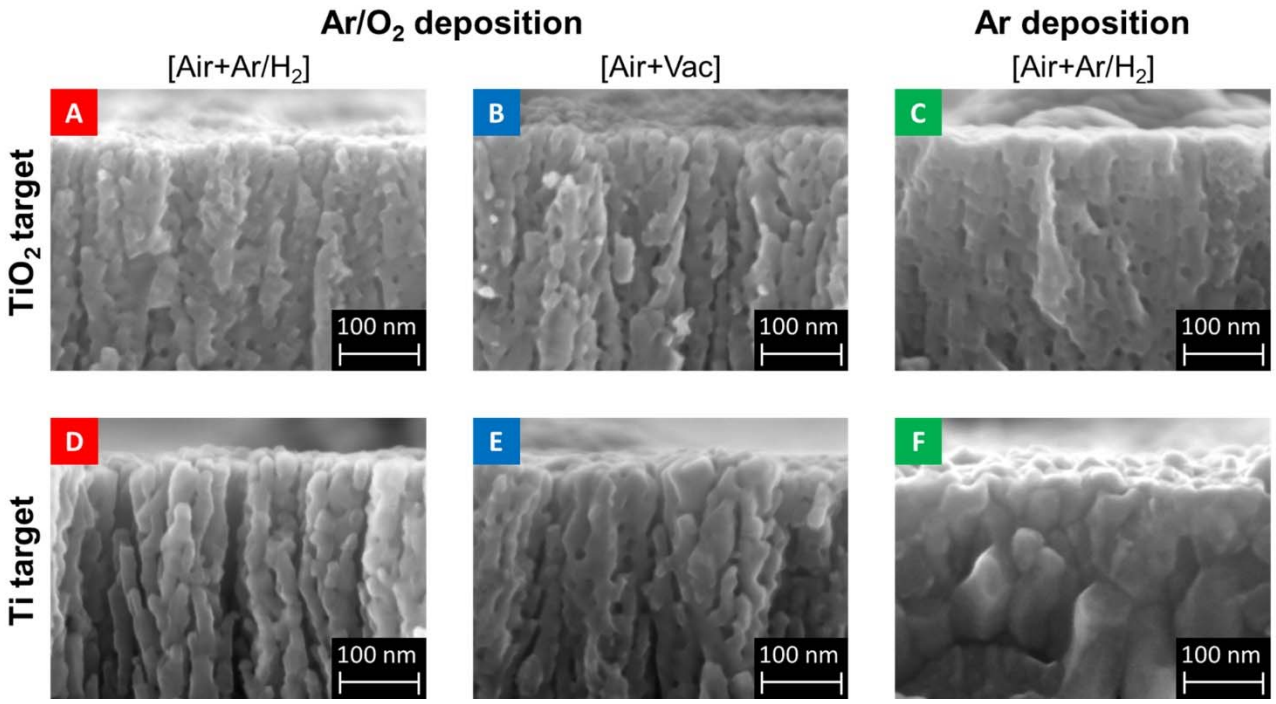

Figure 6: SEM images of TiO_2 films deposited from TiO_2 target (first row) and from Ti target (second row). **A)** Ar/O_2 (50:50)-TiO_2-[Air+Ar/H_2]; **B)** Ar/O_2 (50:50)-TiO_2-[Air+Vac]; **C)** Ar-TiO_2-[Air+Ar/H_2]; **D)** Ar/O_2 (25:75)-Ti-[Air+Ar/H_2]; **E)** Ar/O_2 (25:75)-Ti-[Air+Vac]; **F)** Ar-Ti-[Air+Ar/H_2].

For the Ar/O_2 (25:75)-Ti-[Air+Ar/H_2], i.e. the most photoactive film, a more detailed morphological analysis with high resolution TEM images was carried out, comparing this film with the [Air]-annealed one (Fig. 7). Both the [Air]-annealed film (Fig. 7A) and the [Air+Ar/H_2]-annealed one consist of an assembly of nanocrystals with approximate size of tens of nm; however, the [Air+Ar/H_2]-annealed film shows apparently larger crystals having a more regular shape and surfaces; this effect can be ascribed to the second annealing step experienced by the [Air+Ar/H_2]-annealed film.

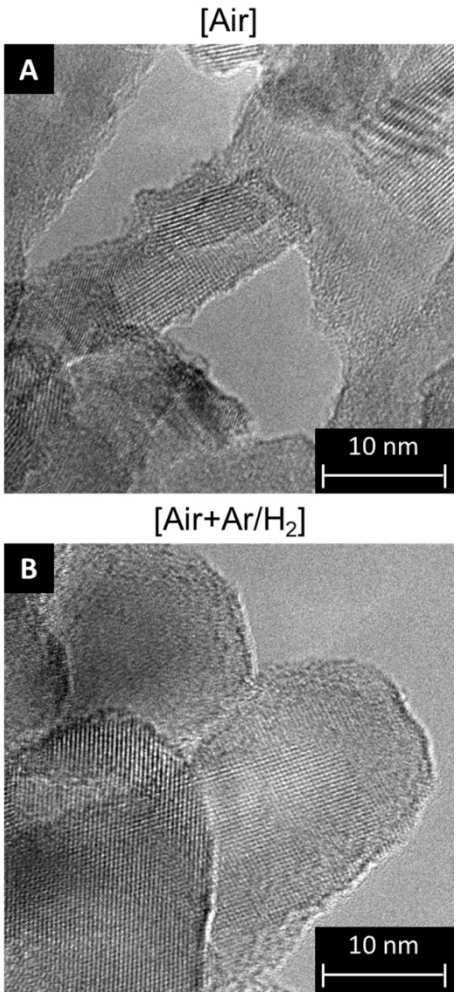

Figure 7: TEM images of annealed Ar/O_2 (25:75)-Ti. **A)** [Air]; **B)** [Air+Ar/H_2].

The crystalline structure of annealed TiO_2 films was evaluated by Raman spectroscopy and X-ray diffraction, as presented in Fig. 8 (as-deposited films in these experimental conditions are amorphous, as already discussed in ref. [32]). In Raman spectra, the photoluminescence background has been removed for the sake of clarity (the occurrence of this background was already discussed in our previous work [32] and was ascribed to defect levels in the bandgap induced by the reducing treatment).

Fig. 8A shows spectra of the films presented in Figs. 6A–C, i.e. deposited from TiO_2 target; the five characteristic peaks of anatase phase at 144, 198, 399, 517 and 639 cm^{-1} are present in all the spectra, irrespectively of the annealing process ([Air+Ar/H_2] vs. [Air+Vac] for Ar/O_2 (50:50)-TiO_2 film) as well as of the deposition gas choice (Ar/O_2 (50:50)-TiO_2 vs. Ar-TiO_2, both with [Air+Ar/H_2] annealing). This effect confirms our previous observations on similar TiO_2 films [32]. Fig. 8B, on the other hand, shows Raman spectra of the films presented in Figs. 6D−F, i.e. deposited from Ti target. In this case, the Ar/O_2 (25:75)-Ti films with [Air+Ar/H_2] annealing and with [Air+Vac] annealing still show the characteristic Raman spectrum of anatase, with no evident peak shift or broadening, similarly to films deposited from TiO_2 target; instead, the Ar-Ti-[Air+Ar/H_2] film is characterized by weak and broad Raman peaks, corresponding to a mixture of anatase and rutile phase (see the rutile E_g and A_{1g} peaks at 440 cm^{-1} and 610 cm^{-1}, respectively) [60] with a large degree of disorder and consistent with a partially oxidized film. This observation

can be related to the fact that the deposition of Ar-Ti film occurs in the absence of oxygen (apart from possible impurities), so that the as-deposited film is metallic and undergoes partial oxidation during the annealing process.

The structural information gained with Raman spectroscopy has been confirmed with XRD measurements, as shown in Figs. 8C and 8D. Most of the investigated films, indeed, exhibit the presence of the anatase phase, with a crystal domain size, estimated through the Scherrer formula for the (004) peaks, between 30 and 40 nm (see Table S1); in addition, no evident peak shift is present, confirming a good crystallinity of the material. On the contrary, the Ar-Ti-[Air+Ar/H_2] film, shows very weak and broadened peaks, corresponding to both anatase and rutile phases, but the low signal/noise ratio prevents the evaluation of a crystallite size in this case; this is consistent with a strongly under-oxidized and disordered material.

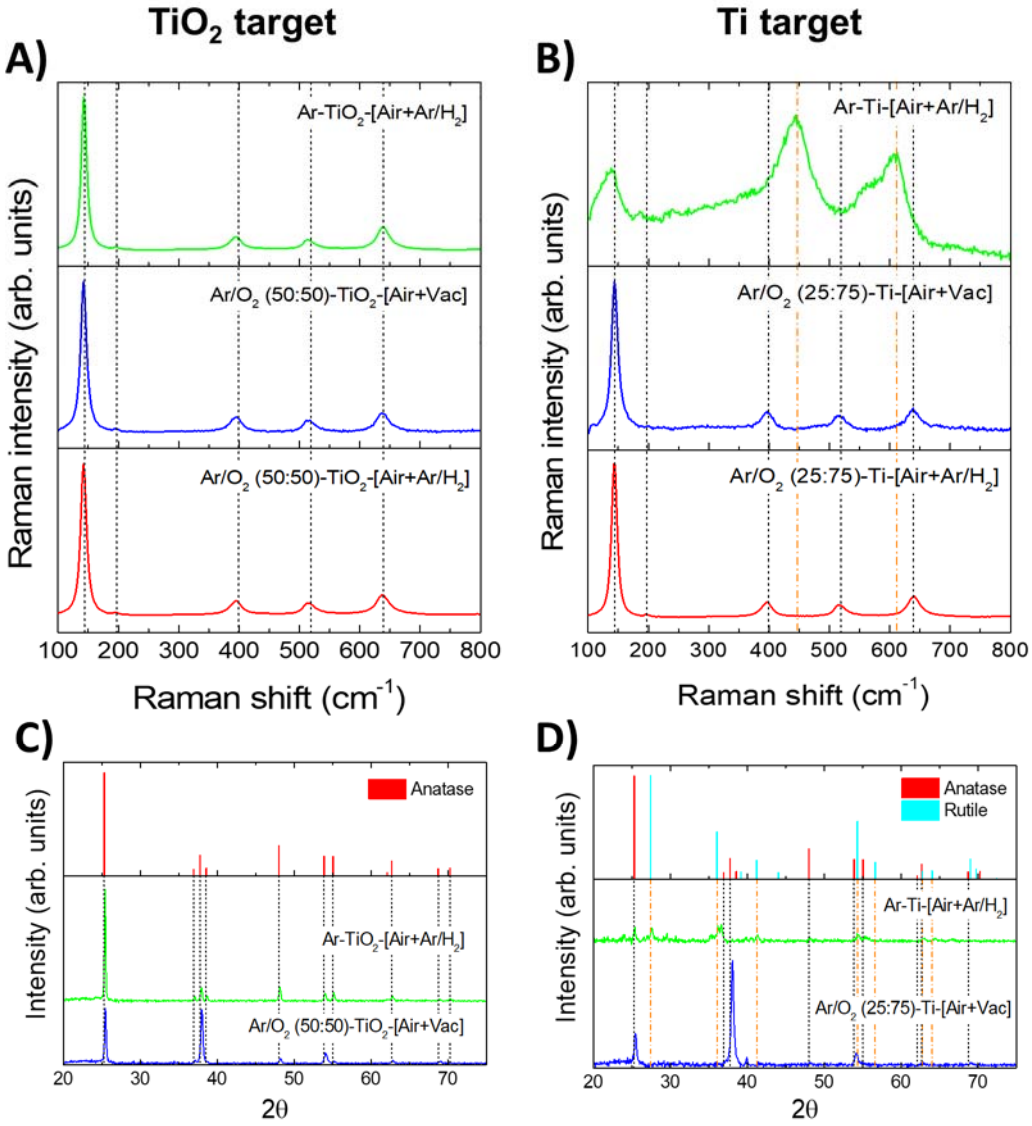

Figure 8: Structural characterization of annealed TiO_2 films: Raman spectra (**A** and **B**) and XRD patterns (**C** and **D**) of films deposited from TiO_2 target (**A** and **C**) and from Ti target (**B** and **D**). Vertical dotted lines (black) and dashed-dotted lines (orange) are also reported as reference to anatase and rutile peaks, respectively (XRD anatase and rutile reference spectra, on top of **C** and **D**, have been taken from a database [61]).

The optical properties of the optimal depositions (see Fig. 3A) were investigated with transmittance and reflectance spectra in the UV-vis-NIR region (Fig. 9; the inset shows the absorbance profile). Considering the Ar/O_2 (50:50)-TiO_2 film (Fig. 9A), it can be observed that both the [Air+Ar/H_2]- and [Air+Vac]-annealed films show an absorption tail extending into the visible range (see inset). Evaluating the mean transmittance in the visible range (400 – 700 nm), for the two mentioned films one obtains T_{vis} = 79.6% and 75.0%. A similar behavior is observed for films deposited by ablation of the Ti target, i.e. Ar/O_2 (25:75)-Ti (Fig. 9B). In general, the visible transmittance T_{vis} is lower for films deposited with Ti target, i.e. about 73.6% for the [Air+Ar/H_2] annealed one and 71.2% for the [Air+Vac] annealed one. Finally, the bandgap of all the mentioned films, evaluated with the Tauc plot method from transmittance and reflectance spectra in the 290-600 nm region (Figs. S3 and S4, see Supporting information), does not differ from the typical value of anatase (3.2 eV).

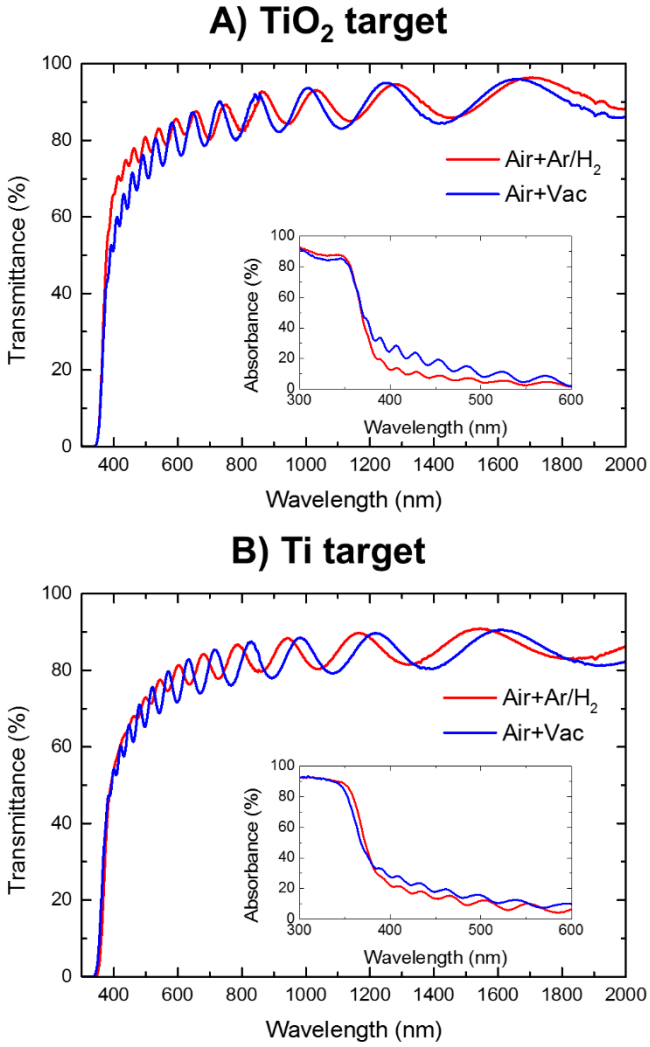

Figure 9: Optical analysis of annealed Ar/O_2 (50:50)-TiO_2 **(A)** and Ar/O_2 (25:75)-Ti films **(B)** (red: [Air+Ar/H_2]; blue: [Air+Vac]).

3.3 Discussion

Two sets of symmetric PLD experiments were performed, i.e. ablation from TiO_2 and Ti targets in background atmospheres with constant pressure and different O_2 content, from pure O_2 to pure Ar, followed by different thermal treatments in oxidizing and reducing conditions; we were thus able to study in detail the effects of the preparation parameters on the final photoresponse of TiO_2

photoanodes tested in a PEC water splitting cell. For selected films (the most photoactive ones), the effect of annealing in vacuum, as alternative reducing atmosphere to Ar/H_2, was also considered to improve the material photoactivity after the standard air annealing.

First, we discuss the effects of $Air+Ar/H_2$ annealing. As a general remark, several defects can be formed in hydrogen-treated TiO_2 depending on the annealing conditions, also leading to different effects on different forms of TiO_2 nanomaterials [9,10]; this is also suggested by theoretical studies [62–65]. Considering mainly Ar/H_2 annealing at atmospheric pressure, it is reported that it leads to the formation of oxygen vacancies (V_O)/Ti^{3+} sites and/or a surface disordered layer on rutile 1D nanostructures [51,54,55]; Wang et al. [53], in addition, report that annealing rutile nanowires in N_2/H_2 atmosphere increases their donor density (by means of V_O). An increase in electrical conductivity in anatase nanotubes after Ar/H_2 annealing is also suggested by different authors [52,66,67], which is favorable for a thin film in a PEC arrangement. Liu and coworkers, however, compare the Ar/H_2 annealing with a high-pressure pure H_2 treatment and show that only the latter leads to open-circuit photocatalytic activity without the need of a co-catalyst, which is ascribed to paramagnetic Ti^{3+} defects acting as intrinsic co-catalytic centers [52]; in the seminal work on *black titania* by Chen and coworkers, however, a Pt co-catalyst on hydrogenated anatase nanoparticles was still employed in photocatalytic tests [68]. Differently, surface disorder, but with the presence of bridging −OH sites rather than Ti^{3+}, has been reported by Li *et al.* [69] in rutile ultra-small nanoparticles without any hydrogenation treatment, leading to bandgap narrowing and visible-light photocatalytic activity.

In our case, annealing in Ar/H_2 atmosphere generally improves the photoresponse of the [Air]-annealed photoanodes tested in this study (Fig. 3A), consistently with our previous work [32]. However, defects are hardly detectable by our investigations and, moreover, they are still a debated issue in the literature, as briefly pointed out above. For this reason, it is out of the scope of this work to study the precise atomistic effect of hydrogen annealing, but we can hypothesize that a surface disorder/defectivity can explain the general photocurrent improvement from the [Air]-annealed photoanodes to the [$Air+Ar/H_2$]-annealed ones in this study, similarly as in our previous one [32]. This is supported by the increase of quantum efficiency in the UV range [32], as reported also in other works [31,50,67,70].

In the following, we discuss the effects of the deposition conditions on the photoelectrochemical response of photoanodes. For the films deposited in pure Ar, a more compact morphology is observed (see Figs. 6C and 6F) and a lower oxygen content is expected, which does not prevent the formation of a crystalline anatase phase for the Ar-TiO_2-[$Air+Ar/H_2$] film (see Figs. 8A-C) but leads to a less ordered structure for the Ar-Ti film (see Figs. 8B-D), which, moreover, has zero transmittance (not shown). These observations can suggest an excessive amount of defects in the material, which in turn can account for the moderately low efficiency of these photoanodes. Considering, instead, all the Ar/O_2-TiO_2-[$Air+Ar/H_2$] films, it can be observed that they show an increased photoresponse with respect to the ones deposited in pure O_2 (O_2-TiO_2) or in pure Ar (Ar-TiO_2), confirming our previous findings on Ar/O_2 deposition [32]. Moreover, a clear trend is observed, as the maximum photoconversion efficiency is measured for the Ar/O_2 (50:50)-TiO_2-[$Air+Ar/H_2$] photoanode (see Fig. 3A). A similar effect appears also for all the Ar/O_2-Ti-[$Air+Ar/H_2$] films, but in this case the optimum is found in correspondence to a higher percentage

of oxygen in the deposition background gas mixture, i.e. Ar/O_2 (25:75)-Ti film, and the pure O_2 deposition shows a high photocurrent. These findings can be discussed by considering the deposition process: the oxygen content in the film is both related to the target material and the background gas mixture in the case of depositions from TiO_2 target, but only to the gas mixture in the case of depositions from Ti target, so a higher concentration of oxygen in the gas is needed in the second case. These results, thus, suggest that some degree of oxygen shortage in the deposition process (and thus a slight oxygen sub-stoichiometry in the film) leads to a better photocatalytic performance, as indicated by our previous investigation [32]. The oxygen-related effect during deposition is not affected by the subsequent first annealing step in [Air], so it is reasonable to expect that it mainly concerns the nanoparticles core (while the hydrogenation step mainly affects the surface, as discussed above). The beneficial effect can be tentatively ascribed to a better conductivity within the slightly reduced material constituting the film [71].

Finally, we considered the effect of vacuum annealing on the two optimal films, i.e. Ar/O_2 (50:50)-TiO_2 and Ar/O_2 (25:75)-Ti (see Fig. 4). The [Air+Vac] thermal treatment, rather than a "direct" vacuum annealing, was chosen on the basis of other works in literature, such as ref. [33], and of the results of our previous work [32], as a first crystallization and sintering step was fundamental to obtain a final increase in photoresponse. For the Ar/O_2 (50:50)-TiO_2 sample an increase in photoresponse is observed with respect to the [Air]-annealed film; moreover, a higher efficiency for the [Air+Vac]-annealed film with respect to the [Air+Ar/H_2]-annealed film emerges. The opposite occurs for the Ar/O_2 (25:75)-Ti film: the [Air+Vac]-annealed does not substantially differ from the [Air]-annealed one in terms of photoconversion efficiency. While, in the first case, the increase in photoresponse can be motivated with similar arguments as for the [Air+Ar/H_2] annealing, in the second case this effect is unclear. Further investigations are needed to investigate the structural and functional effects of vacuum treatment with respect to hydrogenation.

To summarize, these observations show that the material defectivity can be adjusted by finely tuning the deposition conditions and the annealing treatments, achieving a control on the functional properties, as shown by photocurrent measurements in water splitting cells.

4. Conclusions

The possibility to tune the photoresponse of hierarchical TiO_2 nanostructured films was explored by controlling the synthesis condition, i.e. the material growth parameters with Pulsed Laser Deposition (TiO_2 and Ti targets with Ar/O_2 background gas mixtures) as well as the second annealing step in reducing conditions (following a standard air annealing necessary for crystallization in anatase phase). Since from the morphological and structural point of view no major differences between the films emerge, we suggest that defects related to the deposition or annealing reducing conditions are responsible for the different material photoactivity. The photoresponse dependence on the synthesis process is evident both for the air-annealed films and, particularly, for those annealed in Ar/H_2 mixture, which generally show a higher photoactivity. In particular, two optimal deposition strategies emerge starting from TiO_2 and Ti target, respectively, even though vacuum annealing shows a different effect for these films; further studies should be necessary to address the comprehension of this relevant aspect.

The results presented in this work show that hierarchical TiO_2 nanostructured films with a tunable photoresponse can be obtained by exploiting the versatility of Pulsed Laser Deposition and annealing treatments in Ar/H_2 at atmospheric pressure easily available at the laboratory scale. This suggests the possibility of further optimizing these materials for PEC water splitting applications as well as others, such as photocatalysis, solid-state dye-sensitized solar cells and lithium storage devices.

Acknowledgements

This work was supported by the FARB project of the Department of Energy, Politecnico di Milano.

References

[1] Fujishima A, Honda K. Electrochemical Photolysis of Water at a Semiconductor Electrode. Nature 1972;238:37–8. doi:10.1038/238037a0.

[2] Bak T, Nowotny J, Rekas M, Sorrell CC. Photo-electrochemical hydrogen generation from water using solar energy. Materials-related aspects. Int J Hydrogen Energ 2002;27:991–1022. doi:10.1016/S0360-3199(02)00022-8.

[3] Nowotny J, Bak T, Nowotny MK, Sheppard LR. Titanium dioxide for solar-hydrogen I. Functional properties. Int J Hydrogen Energ 2007;32:2609–29. doi:10.1016/j.ijhydene.2006.09.004.

[4] Chen X, Mao SS. Titanium Dioxide Nanomaterials: Synthesis, Properties, Modifications, and Applications. Chem Rev 2007;107:2891–959. doi:10.1021/cr0500535.

[5] Roy P, Berger S, Schmuki P. TiO2 Nanotubes: Synthesis and Applications. Angew Chem Int Ed 2011;50:2904–39. doi:10.1002/anie.201001374.

[6] Riboni F, Truong Nguyen N, So S, Schmuki P. Aligned metal oxide nanotube arrays: key-aspects of anodic TiO 2 nanotube formation and properties. Nanoscale Horiz 2016;1:445–66. doi:10.1039/C6NH00054A.

[7] Kharisov BI, Kharissova OV, García BO, Méndez YP, de la Fuente IG. State of the art of nanoforest structures and their applications. RSC Adv 2015;5:105507–23. doi:10.1039/C5RA22738K.

[8] Chen HM, Chen CK, Liu R-S, Zhang L, Zhang J, Wilkinson DP. Nano-architecture and material designs for water splitting photoelectrodes. Chem Soc Rev 2012;41:5654–71. doi:10.1039/C2CS35019J.

[9] Chen X, Liu L, Huang F. Black titanium dioxide (TiO2) nanomaterials. Chem Soc Rev 2015;44:1861–85. doi:10.1039/C4CS00330F.

[10] Liu X, Zhu G, Wang X, Yuan X, Lin T, Huang F. Progress in Black Titania: A New Material for Advanced Photocatalysis. Adv Energy Mater 2016;6:1600452. doi:10.1002/aenm.201600452.

[11] Warren SC, Thimsen E. Plasmonic solar water splitting. Energy Environ Sci 2012;5:5133–46. doi:10.1039/C1EE02875H.

[12] Cacciato G, Zimbone M, Ruffino F, Grimaldi MG. TiO2 Nanostructures and Nanocomposites for Sustainable Photocatalytic Water Purification. In: Larramendy ML, Soloneski S, editors. Green Nanotechnology - Overview and Further Prospects, InTech; 2016.

[13] Nguyen NT, Altomare M, Yoo JE, Taccardi N, Schmuki P. Noble Metals on Anodic TiO2 Nanotube Mouths: Thermal Dewetting of Minimal Pt Co-Catalyst Loading Leads to Significantly Enhanced Photocatalytic H2 Generation. Adv Energy Mater 2016;6:1501926. doi:10.1002/aenm.201501926.

[14] Li A, Wang T, Chang X, Cai W, Zhang P, Zhang J, et al. Spatial separation of oxidation and reduction co-catalysts for efficient charge separation: Pt@TiO2@MnOx hollow spheres for photocatalytic reactions. Chem Sci 2016;7:890–5. doi:10.1039/C5SC04163E.

[15] Zhang P, Wang T, Gong J. Passivation of surface states by ALD-grown TiO2 overlayers on Ta3N5 anodes for photoelectrochemical water oxidation. Chem Commun 2016;52:8806–9. doi:10.1039/C6CC03411J.

[16] Ros C, Andreu T, Hernández-Alonso MD, Penelas-Pérez G, Arbiol J, Morante JR. Charge Transfer Characterization of ALD-Grown TiO2 Protective Layers in Silicon Photocathodes. ACS Appl Mater Interfaces 2017;9:17932–41. doi:10.1021/acsami.7b02996.

[17] Li J, G. Hoffmann MW, Shen H, Fabrega C, Daniel Prades J, Andreu T, et al. Enhanced photoelectrochemical activity of an excitonic staircase in CdS@TiO 2 and CdS@anatase@rutile TiO 2 heterostructures. J Mater Chem A 2012;22:20472–6. doi:10.1039/C2JM33404F.

[18] Han H, Riboni F, Karlicky F, Kment S, Goswami A, Sudhagar P, et al. α-Fe2O3/TiO2 3D hierarchical nanostructures for enhanced photoelectrochemical water splitting. Nanoscale 2017;9:134–42. doi:10.1039/C6NR06908H.
[19] Gong J, Luo Z, Wang T, Zhang J, Li C, Li H. Dendritic Hematite Nanoarray Photoanode Modified by Conformal Titanium Dioxide Interlayer for Effective Charge Collection. Angew Chem Int Ed n.d.:n/a-n/a. doi:10.1002/anie.201705772.
[20] Eftekhari A, Babu VJ, Ramakrishna S. Photoelectrode nanomaterials for photoelectrochemical water splitting. Int J Hydrogen Energ 2017;42:11078–109. doi:10.1016/j.ijhydene.2017.03.029.
[21] Kment S, Riboni F, Pausova S, Wang L, Wang L, Han H, et al. Photoanodes based on TiO2 and α-Fe2O3 for solar water splitting – superior role of 1D nanoarchitectures and of combined heterostructures. Chem Soc Rev 2017;46:3716–69. doi:10.1039/C6CS00015K.
[22] Eason R, editor. Pulsed Laser Deposition of Thin Films: Applications-Led Growth of Functional Materials. John Wiley & Sons; 2007.
[23] Casari CS, Li Bassi A. Pulsed Laser Deposition of Nanostructured Oxides: from Clusters to Functional Films. In: Arkin WT, editor. Advances in Laser and Optics Research. Volume 7, Nova Science Publishers; 2011, p. 65–100.
[24] Sauvage F, Di Fonzo F, Li Bassi A, Casari CS, Russo V, Divitini G, et al. Hierarchical TiO2 Photoanode for Dye-Sensitized Solar Cells. Nano Lett 2010;10:2562–7. doi:10.1021/nl101198b.
[25] Noh JH, Park JH, Han HS, Kim DH, Han BS, Lee S, et al. Aligned Photoelectrodes with Large Surface Area Prepared by Pulsed Laser Deposition. J Phys Chem C 2012;116:8102–10. doi:10.1021/jp211233s.
[26] Passoni L, Ghods F, Docampo P, Abrusci A, Martí-Rujas J, Ghidelli M, et al. Hyperbranched Quasi-1D Nanostructures for Solid-State Dye-Sensitized Solar Cells. ACS Nano 2013;7:10023–31. doi:10.1021/nn403979h.
[27] Di Fonzo F, Casari CS, Russo V, Brunella MF, Li Bassi A, Bottani CE. Hierarchically organized nanostructured TiO2 for photocatalysis applications. Nanotechnology 2009;20:015604. doi:10.1088/0957-4484/20/1/015604.
[28] Matarrese R, Nova I, Li Bassi AL, Casari CS, Russo V. Hierarchical nanostructured TiO2 films prepared by reactive pulsed laser position for photoelectrochemical water splitting. Chem Eng Trans 2014;41:313–318. doi:10.3303/CET1441053.
[29] Matarrese R, Palmas S, Nova I, Li Bassi A, Casari CS, Russo V, et al. Photoelectrochemical Characterization of Hierarchical TiO2 Nanoarchitectures Obtained by Reactive Pulsed Laser Deposition (PLD). Chem Eng Trans 2014;41:397–402. doi:10.3303/CET1441067.
[30] Matarrese R, Nova I, Li Bassi A, Casari CS, Russo V, Palmas S. Preparation and optimization of TiO2 photoanodes fabricated by pulsed laser deposition for photoelectrochemical water splitting. J Solid State Electrochem 2017:1–16. doi:10.1007/s10008-017-3639-7.
[31] Wang G, Wang H, Ling Y, Tang Y, Yang X, Fitzmorris RC, et al. Hydrogen-Treated TiO2 Nanowire Arrays for Photoelectrochemical Water Splitting. Nano Lett 2011;11:3026–33. doi:10.1021/nl201766h.
[32] Mascaretti L, Ferrulli S, Mazzolini P, Casari CS, Russo V, Matarrese R, et al. Hydrogen-treated hierarchical titanium oxide nanostructures for photoelectrochemical water splitting. Sol Energy Mater Sol Cells 2017;169:19–27. doi:10.1016/j.solmat.2017.04.045.
[33] Xia T, Zhang Y, Murowchick J, Chen X. Vacuum-treated titanium dioxide nanocrystals: Optical properties, surface disorder, oxygen vacancy, and photocatalytic activities. Catal Today 2014;225:2–9. doi:10.1016/j.cattod.2013.08.026.
[34] Chen B, Beach JA, Maurya D, Moore RB, Priya S. Fabrication of black hierarchical TiO2 nanostructures with enhanced photocatalytic activity. RSC Adv 2014;4:29443–9. doi:10.1039/C4RA04260C.

[35] Scherrer P. Bestimmung der Größe und der inneren Struktur von Kolloidteilchen mittels Röntgenstrahlen. Göttinger Nachrichten Math Phys 1918;2:98–100.
[36] Palmas S, Polcaro AM, Ruiz JR, Da Pozzo A, Mascia M, Vacca A. TiO2 photoanodes for electrically enhanced water splitting. Int J Hydrogen Energ 2010;35:6561–70. doi:10.1016/j.ijhydene.2010.04.039.
[37] Palmas S, Pozzo AD, Mascia M, Vacca A, Matarrese R, Nova I. Photo-electrochemical behavior at different wavelengths of electrochemically obtained TiO2 nanotubes. J Appl Electrochem 2012;42:745–51. doi:10.1007/s10800-012-0456-7.
[38] Lucas-Granados B, Sánchez-Tovar R, Fernández-Domene RM, García-Antón J. Study of the annealing conditions and photoelectrochemical characterization of a new iron oxide bi-layered nanostructure for water splitting. Sol Energy Mater Sol Cells 2016;153:68–77. doi:10.1016/j.solmat.2016.04.005.
[39] Fernández-Domene RM, Sánchez-Tovar R, Segura-Sanchís E, García-Antón J. Novel tree-like WO3 nanoplatelets with very high surface area synthesized by anodization under controlled hydrodynamic conditions. Chem Eng J 2016;286:59–67. doi:10.1016/j.cej.2015.10.069.
[40] Cong Y, Chen M, Xu T, Zhang Y, Wang Q. Tantalum and aluminum co-doped iron oxide as a robust photocatalyst for water oxidation. Appl Catal B-Environ 2014;147:733–40. doi:10.1016/j.apcatb.2013.10.009.
[41] Huang M-C, Chang W-S, Lin J-C, Chang Y-H, Wu C-C. Magnetron sputtering process of carbon-doped α-Fe2O3 thin films for photoelectrochemical water splitting. J Alloy Compd 2015;636:176–82. doi:10.1016/j.jallcom.2015.02.166.
[42] Sánchez-Tovar R, Fernández-Domene RM, García-García DM, García-Antón J. Enhancement of photoelectrochemical activity for water splitting by controlling hydrodynamic conditions on titanium anodization. J Power Sources 2015;286:224–31. doi:10.1016/j.jpowsour.2015.03.174.
[43] Varghese OK, Grimes CA. Appropriate strategies for determining the photoconversion efficiency of water photoelectrolysis cells: A review with examples using titania nanotube array photoanodes. Sol Energy Mater Sol Cells 2008;92:374–84. doi:10.1016/j.solmat.2007.11.006.
[44] Zhou B, Schulz M, Lin HY, Shah SI, Qu J, Huang CP. Photoeletrochemical generation of hydrogen over carbon-doped TiO2 photoanode. Appl Catal B-Environ 2009;92:41–9. doi:10.1016/j.apcatb.2009.07.026.
[45] Cowan AJ, Tang J, Leng W, Durrant JR, Klug DR. Water Splitting by Nanocrystalline TiO2 in a Complete Photoelectrochemical Cell Exhibits Efficiencies Limited by Charge Recombination. J Phys Chem C 2010;114:4208–14. doi:10.1021/jp909993w.
[46] Spadavecchia F, Ardizzone S, Cappelletti G, Falciola L, Ceotto M, Lotti D. Investigation and optimization of photocurrent transient measurements on nano-TiO2. J Appll Electrochem 2013;43:217–25. doi:10.1007/s10800-012-0485-2.
[47] Song X-M, Wu J-M, Tang M-Z, Qi B, Yan M. Enhanced Photoelectrochemical Response of a Composite Titania Thin Film with Single-Crystalline Rutile Nanorods Embedded in Anatase Aggregates. J Phys Chem C 2008;112:19484–92. doi:10.1021/jp8076886.
[48] Xu Z, Yu J. Visible-light-induced photoelectrochemical behaviors of Fe-modified TiO2 nanotube arrays. Nanoscale 2011;3:3138–44. doi:10.1039/C1NR10282F.
[49] Zhang K, Shi X-J, Kim JK, Park JH. Photoelectrochemical cells with tungsten trioxide/Mo-doped BiVO4 bilayers. Phys Chem Chem Phys 2012;14:11119–24. doi:10.1039/C2CP40991G.
[50] Hoang S, Berglund SP, Hahn NT, Bard AJ, Mullins CB. Enhancing Visible Light Photo-oxidation of Water with TiO2 Nanowire Arrays via Cotreatment with H2 and NH3: Synergistic Effects between Ti3+ and N. J Am Chem Soc 2012;134:3659–62. doi:10.1021/ja211369s.

[51] Zhang S, Zhang S, Peng B, Wang H, Yu H, Wang H, et al. High performance hydrogenated TiO2 nanorod arrays as a photoelectrochemical sensor for organic compounds under visible light. Electrochem Commun 2014;40:24–7. doi:10.1016/j.elecom.2013.12.013.
[52] Liu N, Schneider C, Freitag D, Hartmann M, Venkatesan U, Müller J, et al. Black TiO2 Nanotubes: Cocatalyst-Free Open-Circuit Hydrogen Generation. Nano Lett 2014;14:3309–13. doi:10.1021/nl500710j.
[53] Wang D, Zhang X, Sun P, Lu S, Wang L, Wang C, et al. Photoelectrochemical Water Splitting with Rutile TiO2 Nanowires Array: Synergistic Effect of Hydrogen Treatment and Surface Modification with Anatase Nanoparticles. Electrochim Acta 2014;130:290–5. doi:10.1016/j.electacta.2014.03.024.
[54] Wang C-C, Chou P-H. Effects of various hydrogenated treatments on formation and photocatalytic activity of black TiO2 nanowire arrays. Nanotechnology 2016;27:325401. doi:10.1088/0957-4484/27/32/325401.
[55] Wang X, Zhang S, Xie Y, Wang H, Yu H, Shen Y, et al. Branched hydrogenated TiO2 nanorod arrays for improving photocatalytic hydrogen evolution performance under simulated solar light. Int J Hydrogen Energ 2016;41:20192–7. doi:10.1016/j.ijhydene.2016.09.029.
[56] Cai J, Wu M, Wang Y, Zhang H, Meng M, Tian Y, et al. Synergetic Enhancement of Light Harvesting and Charge Separation over Surface-Disorder-Engineered TiO2 Photonic Crystals. Chem 2017;2:877–92. doi:10.1016/j.chempr.2017.05.006.
[57] Fusi M, Russo V, Casari CS, Li Bassi A, Bottani CE. Titanium oxide nanostructured films by reactive pulsed laser deposition. Appl Surf Sci 2009;255:5334–7. doi:10.1016/j.apsusc.2008.06.206.
[58] Fusi M, Maccallini E, Caruso T, Casari CS, Li Bassi A, Bottani CE, et al. Surface electronic and structural properties of nanostructured titanium oxide grown by pulsed laser deposition. Surf Sci 2011;605:333–40. doi:10.1016/j.susc.2010.10.039.
[59] Long H, Yang G, Chen A, Li Y, Lu P. Growth and characteristics of laser deposited anatase and rutile TiO2 films on Si substrates. Thin Solid Films 2008;517:745–9. doi:10.1016/j.tsf.2008.08.179.
[60] Li Bassi A, Cattaneo D, Russo V, Bottani CE, Barborini E, Mazza T, et al. Raman spectroscopy characterization of titania nanoparticles produced by flame pyrolysis: The influence of size and stoichiometry. J Appl Phys 2005;98:074305. doi:10.1063/1.2061894.
[61] WWW-MINCRYST - Cristallographic database for minerals n.d. http://database.iem.ac.ru/mincryst/ (accessed June 23, 2017).
[62] Di Valentin C, Pacchioni G, Selloni A. Electronic Structure of Defect States in Hydroxylated and Reduced Rutile TiO2(110) Surfaces. Phys Rev Lett 2006;97:166803. doi:10.1103/PhysRevLett.97.166803.
[63] Di Valentin C, Pacchioni G, Selloni A. Reduced and n-Type Doped TiO2: Nature of Ti3+ Species. J Phys Chem C 2009;113:20543–52. doi:10.1021/jp9061797.
[64] Liu L, Yu PY, Chen X, Mao SS, Shen DZ. Hydrogenation and Disorder in Engineered Black TiO2. Phys Rev Lett 2013;111:065505. doi:10.1103/PhysRevLett.111.065505.
[65] Gerosa M, Bottani CE, Caramella L, Onida G, Di Valentin C, Pacchioni G. Defect calculations in semiconductors through a dielectric-dependent hybrid DFT functional: The case of oxygen vacancies in metal oxides. J Chem Phys 2015;143:134702. doi:10.1063/1.4931805.
[66] Lu Z, Yip C-T, Wang L, Huang H, Zhou L. Hydrogenated TiO2 Nanotube Arrays as High-Rate Anodes for Lithium-Ion Microbatteries. ChemPlusChem 2012;77:991–1000. doi:10.1002/cplu.201200104.
[67] Liu N, Schneider C, Freitag D, Zolnhofer EM, Meyer K, Schmuki P. Noble-Metal-Free Photocatalytic H2 Generation: Active and Inactive “Black” TiO2 Nanotubes and Synergistic Effects. Chem Eur J 2016;22:13810–4. doi:10.1002/chem.201602714.

[68] Chen X, Liu L, Yu PY, Mao SS. Increasing Solar Absorption for Photocatalysis with Black Hydrogenated Titanium Dioxide Nanocrystals. Science 2011;331:746–50. doi:10.1126/science.1200448.
[69] Li L, Yan J, Wang T, Zhao Z-J, Zhang J, Gong J, et al. Sub-10 nm rutile titanium dioxide nanoparticles for efficient visible-light-driven photocatalytic hydrogen production. Nat Commun 2015;6:5881. doi:10.1038/ncomms6881.
[70] Cui H, Zhao W, Yang C, Yin H, Lin T, Shan Y, et al. Black TiO2 nanotube arrays for high-efficiency photoelectrochemical water-splitting. J Mater Chem A 2014;2:8612–6. doi:10.1039/C4TA00176A.
[71] Mazzolini P, Gondoni P, Russo V, Chrastina D, Casari CS, Li Bassi A. Tuning of Electrical and Optical Properties of Highly Conducting and Transparent Ta-Doped TiO2 Polycrystalline Films. J Phys Chem C 2015;119:6988–97. doi:10.1021/jp5126156.